

Highly efficient adsorption and removal bio-staining dye from industrial wastewater onto mesoporous Ag-MOFs

Meshari M. Aljohani ^a, Salhah D. Al-Qahtani ^b, Mubark Alshareef ^c, Mohamed G. El-Desouky ^{d,*}, Ashraf A. El-Binary ^e, Nashwa M. El-Metwaly ^f, Mohamed A. El-Binary ^g

^a Department of Chemistry, College of Science, University of Tabuk, 71474 Tabuk, Saudi Arabia

^b Department of Chemistry, College of Science, Princess Nourah bint Abdulrahman University, P.O. Box 84428, Riyadh 11671, Saudi Arabia

^c Department of Chemistry, Faculty of Applied Science, Umm-Al-Qura University, Makkah, Saudi Arabia

^d Egyptian Propylene and Polypropylene Company, Port Said 42511, Egypt

^e Chemistry Department, Faculty of Science, Damietta University, Damietta 34517, Egypt

^f Department of Chemistry, Faculty of Science, Mansoura University, El-Gomhoria Street, 35516, Egypt

^g Basic Science Department, Higher Institute of Engineering and Technology, Damietta 34517, Egypt

ARTICLE INFO

Keywords:

Ag-MOF
Batch adsorption
Isotherm
Thermodynamics
Mechanism of interaction
Box-Behnken design

ABSTRACT

Adsorption is an effective and promising approach for removing pollutants from wastewater. Too many hazardous colors were unintentionally released into the water, which had a negative impact on the environment. A popular textile dye is malachite green (MG). Thus, in this work, an environmentally acceptable inorganic-organic Ag metal-organic framework-based technique to remove colors from industrial water was developed (Ag-MOF). The sorbent was analyzed in the first section of the work using SEM, XPS, XRD, FT-IR, pH_{pzc}, and BET, which confirmed that the Ag-MOF had the BET surface area, is 676 m²/g, which is a significant surface area. In a later stage, the sorption properties of the dye were examined along with the effects of pH, sorbent dosage, temperature, and ionic strength; the sorption isotherms and uptake kinetics were examined: As opposed to the kinetic profile, Isotherm profiles are well-fit by the Langmuir equation and can be modeled by the pseudo-second order rate equation. The outcomes further demonstrated that MG was mostly adsorbed onto Ag-MOF adsorbent by electrostatic attraction forces, hydrogen bonding, ion exchange, and pore filling. 2.25 mmol/g was found to be the greatest adsorption effectiveness of MG onto Ag-MOF adsorbent. (i.e. 809.71 mg/g). Adsorbent dosage, solution pH, temperature, and time were the four adsorption process parameters that were tuned using Box- Behnken design (BBD) in response surface methodology (RSM). The (ΔH°), (ΔS°), and (ΔG°) MG dye was endothermically and spontaneously extracted using Ag-MOF as an adsorbent, according to the specifications. Up to five cycles of adsorption-desorption, the synthesised Ag-MOF adsorbent demonstrates exceptional renderability and cyclability. The produced adsorbent's efficacy for purifying wastewater samples at a laboratory scale was assessed as a proof of concept. Study the mechanism of interaction between the Ag-MOF and MG as it could be take place through π - π interaction, pore filling, H-Bonding or electrostatic interaction. The mesoporous Ag-MOF adsorbent offered a simple and effective way to handle water filtering and industrial wastewater management. According to our research, this work is the first to explain how to remove MG dye from wastewater samples using Ag-MOF adsorbents.

1. Introduction

Recent years have seen an increase in the focus on sustainable resource development among planners, environmental scientists, and decision-makers. Water is the most important renewable natural resource among them due to the fact that it is both an essential part of

life and a key enabler. The majority of the world's drinking water comes from groundwater. Over 1.5 billion people throughout the world receive their drinking water from groundwater, which also supplies about 43 % of all irrigation needs (Garg et al., 2019). Groundwater quality and quantity have declined as a result of rising industrialization, the rapid population growth, and unrestricted freshwater use. Per the statistics,

* Corresponding author.

E-mail addresses: mohamed.eldesoky@EPP-EG.com, ch.moh.gamal@gmail.com (M.G. El-Desouky).

1.2 billion people worldwide lack access to clean water, and 663 million people suffer from contaminated water (Rashid et al., 2019). Water discharged into the ecosystem that has either not been cleaned at all or has only been partially treated causes the majority of surface water and groundwater pollution. Particularly, organic dyes from industrial wastes such as paper, solar cells, leather, plastics, and textiles seriously harm the environment and people's health (Amarasooriya and Kawakami, 2019).

Humans have contaminated a limited number of freshwater resources. The discharge water containing dyes is one of the pollution sources. Dyes are employed as colourants in the manufacturing process in a variety of industries, includes those in the food production, cosmetics, automotive, pharmaceutical, plastics, paint, leather, and textile industries. Each year, these companies create more than 7×10^5 tons of dyes and almost 10,000 different types. Even at low concentrations (1 mg/L), dyes are visible to the human eye. Dye contains hazardous elements that harm aquatic life, natural life, and human life, as well as upset the ecological equilibrium. These industrial discharges are highly colored and have high chemical (COD) and biochemical oxygen demands (BOD) (Lee et al., 1999). Dye types include anionic, cationic, and dispersion dyes. Anionic dyes are divided into three subcategories: reactive, direct, and acid dyes. Basic dyes are another name for cationic dyes. Disperse dyes are not ionic (Gu et al., 2013). The release of dyes has detrimental effects on ecosystems, human health, soil fertility, and marine life since they are genotoxic, mutagenic, and carcinogenic. Diverse techniques are used to treat dye wastewater, including membrane separation procedures, degradation, flocculation, precipitation, and oxidation. While these techniques are effective in removing dye, they are costly for developing nations to implement on a wide scale (Islam and Mostafa, 2018; Gao et al., 2011; Agarwal and Singh, 2017). The adsorption technique is commonly used to remove colours because of its great efficacy and ease of use. Adsorbents used in wastewater treatment, including activated carbon, silica gel, MOF, activated alumina, and others, are expensive and need a challenging regeneration process. This has made it possible to search for novel, simple, and affordable adsorbents with outstanding dye percentage removal (Celik et al., 2021).

Malachite green (MG), $C_{23}H_{25}N_2$, is a cationic dye with numerous commercial and industrial uses, including disinfection in medicine and the treatment of fungal and protozoal infections, particularly in aquaculture (Sallam et al., 2018; El-Subraui et al., 2019). The food business uses MG as a coloring and additive, The industries that use it as a dyeing agent include those that work with leather, silk, wool, cotton, paper, and acrylic. In these businesses, one of the biggest issues is getting MG dye out of the environment (Agarwal and Singh, 2017; Royer et al., 2009; Abdolali et al., 2014). The number of dyes released into waterways has increased due to the strong demand for vibrant hues. Infertility, pulmonary toxicity, and teratogenic consequences from MG exposure are all possible side effects. To avoid unnecessary exposure, it is crucial to remove MG dye from water (Mahmoodi, 2013). The dye's complicated chemical makeup, great resilience to oxidising chemicals, and low chemical and biological precipitation efficacy for this sort of molecule make cleaning difficult. As a result, it is recommended that creating techniques for depolarization from aquatic sources is a worthwhile research area (Adebayo et al., 2014).

In the literature, various techniques for wastewater purification have been published. Due to its environmental friendliness and the affordability of traditional adsorbents, The removal of organic contaminants from water via adsorption has been found to be more successful (Nanotube et al., 2013). However, these materials have a low adsorption capacity as well, necessitating the urgent need for additional adsorbents with high removal capacities.

Numerous promising nanomaterials, particularly metal-organic frameworks, have been the subject of recent research (MOFs), to detect and remove harmful metals and organic dyes from the environment. The superior porosity, vast surface area, and organized structure

of MOFs have been linked to the latter's high removal % of harmful dyes and metals. As a result, MOFs outperform traditional materials in detecting and eliminating harmful heavy metals and organic dyes. Different MOFs with tremendous morphology can be created thanks to the interaction between linker subunits and inorganic metals. In general, the usage of MOFs for sensing and eliminating contaminants benefits from the vast availability of different particular linkers. Because of their stability and improved textural properties, Ag imidazolate frameworks are typically regarded as promising adsorbent materials in order to get rid of organic dyes (Li et al., 2017; El-Sewify et al., 2022).

The bigger surface-to-volume ratio of the smaller silver nanoparticles, which results in a larger area of contact between both the nanoparticles and bacteria, has been investigated in the literature as the reason why smaller silver nanoparticles are much more active than those made of larger size. Smaller Ag-MOF naturally releases more silver ions into the environment than larger ones, which effectively inhibits bacterial development. It was discovered that when Ag-MOF are combined, their inhibition zones are bigger than when the corresponding Ag-MOF is used individually. The uniqueness of our work may be summed up as the creation of inorganic-organic MOFs with high MG dye adsorption capabilities as well as antibacterial and fungal activities through synthesis using a one-pot, environmentally friendly technique. Ag-MOF effectively removes 809.713 mg/g of MG from water and has a surface area of $676.06\text{ m}^2/\text{g}$. Examine how temperature, pH, concentration, dose, and time affect the adsorption reaction, as well as how these factors affect the thermodynamic parameter. This will help you confirm that the adsorption reaction was endothermic and spontaneous. This suggests that as the temperature rises, the rate of elimination increases. Investigation into the mechanisms of adsorption and reaction was extensive. A pseudo-second-order kinetic model and an isothermal Langmuir model were used to simulate the adsorption process. These adsorbents can be reused up to five times and still have a removal efficiency of 82.7 %, making them reusable as well. When the efficiency of MG removal from earlier study was examined, it was found that our adsorbent outperformed the others.

2. Materials and methods

2.1. Materials and instruments

The materials and instruments are given in the Support information.

2.2. Synthesis of Ag-MOF nanoparticles

The silver-based metal-organic frameworks were made by dissolving 0.58 g of AgNO_3 at 3 mL distilled water and 1.64 g of 2-methylimidazole in 25.0 mL of ammonium hydroxide, after complete desolvation mix the two solutions together as in the traditional hydrothermal synthesis method. This reaction mixture was heated at 100 °C in a Teflon autoclave with a 100 mL wall for 24 h (5 °C/min heating rate). The substance was centrifuged, cooled, and then washed three times with deionized water before being dried for a whole night at 80 degrees Celsius.

2.3. Removal and batch studies of the Ag-MOF

To ascertain the ideal adsorption circumstances, MG stock solution was made. Utilizing the stock solution, the dye solution was produced at working concentrations ranging from 2.76×10^{-4} to $2.2 \times 10^{-3}\text{ mmol L}^{-1}$. Stock solutions were prepared with deionized water. Several batch adsorption tests were run in order to explore the adsorption capabilities of Ag-MOF for the elimination of MG dye. The necessary quantity of Ag-MOF adsorbent was added to aqueous solutions containing MG dye in a consistent concentration. After that, the mixture was shaken continuously. After a predetermined amount of time, an aliquot of the solution was taken, centrifuged at 6000 rpm to extract it, and the supernatant was filtering out before being subjected to UV-vis spectroscopy analysis.

The MG level was then measured at 617 nm. These measurements established a 100-minute equilibrium time for MG adsorption onto Ag-MOF. Two distinct samples were taken from various places in order to evaluate the performance of Ag-MOF as an adsorbent in wastewater samples. Distilled water was used to dilute the industrial sample from 25 mL to 250 mL. Optimal conditions were met for stirring 100 mL of the diluted sample with Ag-MOF adsorbent (Ag-MOF of 0.5 g, solution pH of 9, shaking time of 1 h, and temperature of 298 K). The whole outline of the instruments was covered in depth in ([supporting information](#)).

For all batch studies, Aluminum foil was used to coat all sample flasks and tubes to prevent MG from photodegrading ([Hassan et al., 2020](#); [Al-Wasidi et al., 2021](#)). [Eqs. \(1\)](#) and [\(2\)](#) to calculate the extraction yield and quantity of MG adsorbed on Ag-MOF.

$$\%R = \frac{(C_0 - C_t)}{C_0} \times 100 \quad (1)$$

$$q_e = \frac{(C_0 - C_e)V}{M} \quad (2)$$

2.4. BBD experimental design

Each of the three trials in the current investigation has three levels of

three factors, as shown in [Table S1 \(Supplementary material\)](#). In order to identify the ideal circumstances for MG adsorption, the BBD model was applied. The settings listed on the table were chosen as the optimization process's response. [Table S1 \(Supplementary material\)](#) demonstrates the bounds of the independent variables that came from the initial research. With the use of Design Expert 7.0, a total of 17 experiments were created and carried out as batch adsorption tests at random. Analysis of variance (ANOVA) was used as a diagnostic tool to establish the proposed model's suitability. The degree to which the responsive variable's variability can be explained by the independent variables and their interactions is measured by the coefficient of determination (R^2), which assesses the polynomial model's accuracy of fit. Fisher's ' F ' test and ' P ' value (probability) were included in the analysis.

3. Results and discussion

3.1. Characterization of Ag-MOF

The Ag-MOF exhibits a highly crystalline structure, as shown by the XRD data in [Fig. 1\(a\)](#). This is supported by the presence of a prominent peak at 28.16° , this is customary of Ag-organic moiety coordination compounds, as well as minor peaks at 10.9° , 11.8° , 13.04° , 17.1° , and

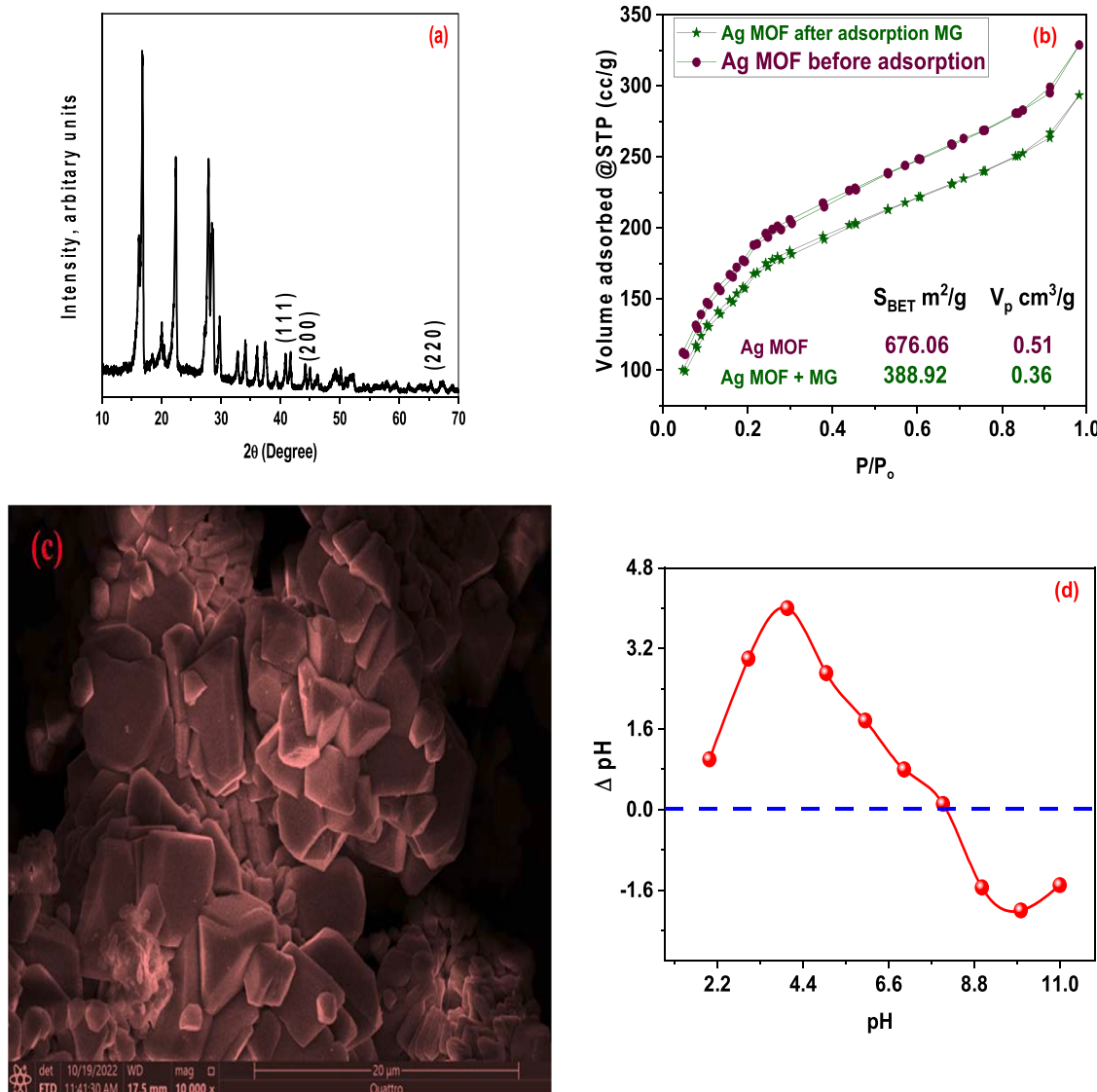


Fig. 1. (a) XRD pattern, (b) N_2 sorption isotherm (c) SEM image of Ag-MOF nanoparticles, and Ag-MOF point of zero charge.

33.97° and the (1 1 1), (2 0 0), (2 2 0) peaks corresponding to 39.16°, 43.84° and 65.31° to Ag-MOF nanoparticles' face-centered cubic crystalline planes (El-Desouky et al., 2021). On other hand, To determine the before and after MG adsorption, pore volume distribution and surface area of Ag-MOF adsorbents, N₂ adsorption-desorption isotherms were developed Fig. 1(b). Our findings support the creation of MG@Ag-MOF after MG adsorption and the production of Ag MOF adsorbents with

microporous holes. The adsorption/desorption isotherms' type II characteristic reflects their sharpness and validates the production of microporous structures and Hysteresis loops are classified as type H₃ loops. After adsorption, the surface area of Ag MOF decreased dramatically, according to our findings. After adsorption, The Ag-MOF's surface area was calculated to be (388.92) m²/g, this is less than the 676.06 m²/g of pure Ag-MOF. Additionally, the pore volume of spent

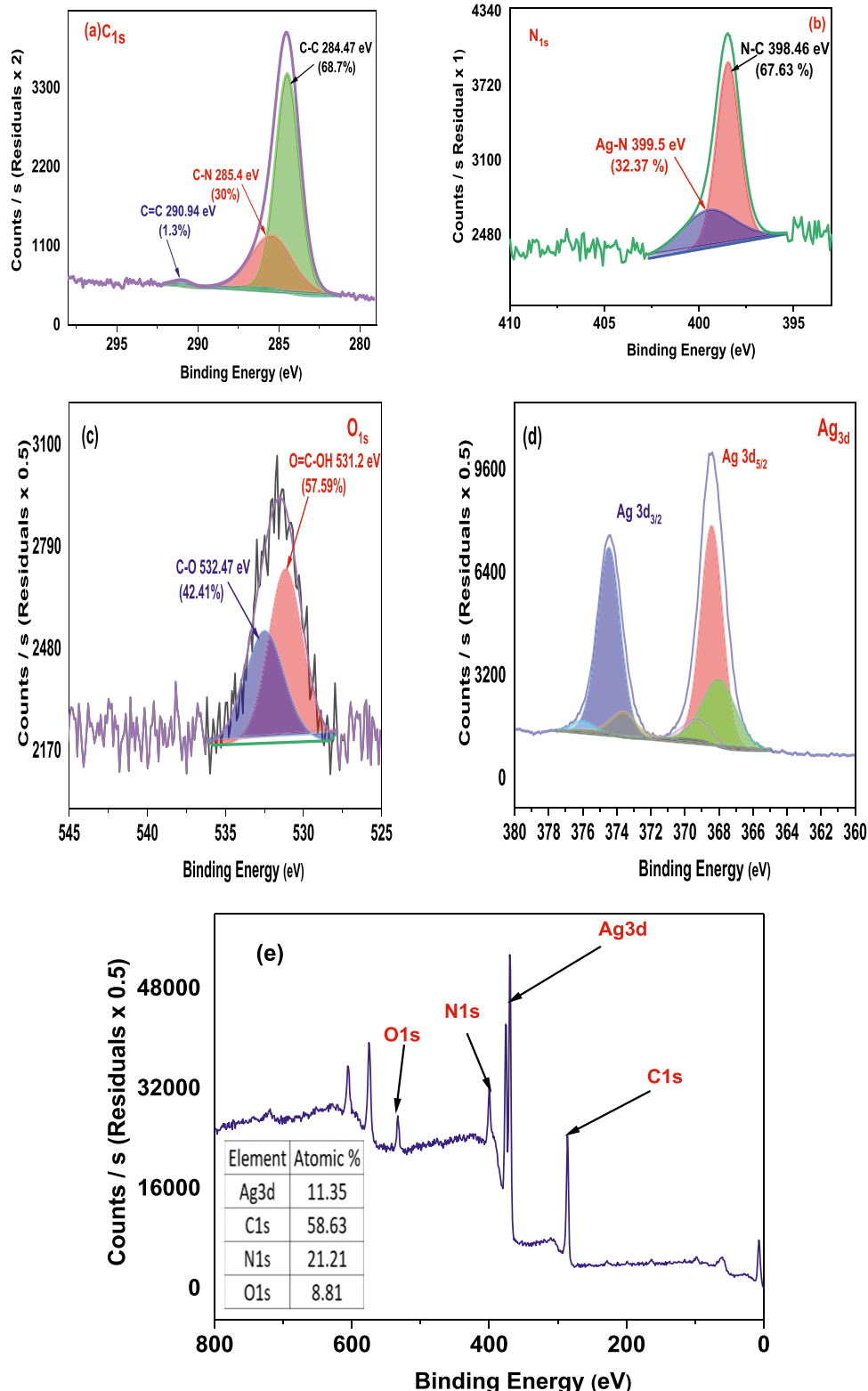


Fig. 2. XPS spectra of the Ag-MOF.

Ag-MOF was lower than that of fresh Ag-MOF. The uptake of MG around the Ag-MOF as well as inside their microporous cages was also displayed, demonstrating the homogeneous filling of MG into the microporous cavities of the inorganic-organic Ag-MOF (Hassan et al., 2020; Al-Wasidi et al., 2021). While, the size and shape of the crystal particles as a result of the reaction conditions were examined using SEM imaging. Area of contact and shape are hugely important factors in medication distribution. Due to Ag-average MOF's diameter ranging from 38.6 to 58 nm, the SEM investigation verified that it was a nanoparticle (Fig. 1(c)). This value demonstrated the formation of microclusters of nanoparticles. There is a good likelihood that MG adsorption will become caught in Ag-MOF pores due to their abundance (Al-Wasidi et al., 2021). Utilizing the point of zero charge (PZC), the charge of the Ag-surface MOF was investigated for MG elimination. The pH_{PZC} value is a critical metric. According to our investigation, the pH_{PZC} of the Ag-MOF is 8.08. The Ag-MOF's functional groups were protonated at a pH of less than pH_{PZC} below pH_{PZC}, the highest adsorption capacity was reported (Arjmand et al., 2020). Fig. 1(d) represented the pH_{PZC} as at the X-axis the initial pH and Y-axis represented the difference between pH_{final} - pH_{initial}.

With the use of a complementary method like XPS, the δ-phase of Ag-MOF is further investigated. This can offer important details on the oxidation states and chemical bonds between the elements. Fig. 2 shows core energy levels of the pure Ag-MOF' Ag 3d state, C 1s, N 1s and O 1s states. The Ag 3d spectrum has shown two peaks related to the Ag 3d5/2 and Ag 3d3/2 core energy levels (due to the spin-orbit coupling), whose binding energies (B.E.) are 368.47 eV and 374.4 eV, respectively (Fig. 2). In O 1s spectrum (Fig. 2), we have observed two peaks at 531.2 eV and 532.4 eV energy positions, which are of oxygen in O=C-OH and C-O phases, respectively (Wang et al., 2017; El-Desouky et al., 2021).

The core energy levels of Ag-MOF (Fig. 2) showed at a little high affinity energy than those described in the literature, which is our main finding from the XPS data (Fuggle et al., 1977). The difficulty in understanding X-ray emission from metals, in which the 'd' energy bands are located a few electronvolts slightly below the Fermi energy level, is the cause of this difference. After alloying the Ag-MOF, the core energy level peaks showed a shift to the higher energy side (Fig. 2). This shows that, when compared to simple ionic compounds, the electron density at an atomic site is lower. This B.E. shift could also result from the partial chemical absorption of species or oxides onto surfaces, which can alter the electronic conditions surrounding the Ag atoms. In addition, the Ag-d-band MOF's photoemission spectra are seen to be smaller than those of ordinary Ag (Fig. 2) (Prabhu et al., 2019). Sample charge is the cause of spectral changes in XPS. The binding energies of photo emitted electrons are shifted as a result of the buildup of positive charges left behind by photoelectrons that are generated from the sample surface. One uses the reference binding energies of silver and, more frequently, carbon to charge-correct a spectrum. Due to the fact that C is present as adsorbed carbon on every XPS sample that we test, the standard uncharged BE of C1S is 284.8, it is regarded as a reference. This indicates that the C 1s peak at 284.8 eV must be used to charge-correct the BE along axis, and once corrected, all other peaks in the same spectrum are similarly rectified. One only needs to keep in mind the C 1s shift and apply it to other peaks, like in our instance, in a different spectrum 284.8–284.47 = 0.33 eV. In order to adjust for all peaks, it should relocate it by 0.33 eV (Kim et al., 2021).

3.2. Optimization adsorption of MG@Ag-MOF by RSM approach

When MG was removed using Ag-MOF, Response Surface Methodology (RSM) was used to determine the interactive impacts of three independent parameters, namely pH, initial MG concentration, and Dose. The selected response was the biosorption capacity (q_e). For the RSM-BBD, a three-factor, three-level design resulted in a total of 17 experimental runs, as shown in Table S1 (Supplementary material).

With a 95 % degree of confidence, the following quadratic relationship (Eq. 3) might be used to forecast the response based on the RSM results:

$$q_e = 1.64 + 0.0432A + 0.07970B + 0.0049C + 0.0271AB + 0.0026AC + 0.0678 BCE - 0.0381A^2 - 0.4833B^2 - 0.0405C^2 \quad (3)$$

3.2.1. ANOVA

In order to confirm the statistical significance of the quadratic model, the regressed data were examined using ANOVA. Table 1 contains the ANOVA findings for the quadratic model's regressed parameters. The relevant term is highly significant, as seen by the bigger F values and lower P-values.

An F-value of 110.75 was found to indicate that the regression model was statistically significant. An F-value this large could only happen owing to noise in 0.01 % of cases. While model terms are significant when the P-value is less than 0.0500. B and B² are important model terms in this instance. Model terms are not significant if the value is higher than 0.1000. The Predicted R² of 0.9394 and the Adjusted R² of 0.9841 are reasonably in agreement.; the difference is less than 0.2. The ratio of signal to noise is measured by Adeq Precision. A ratio of at least 4 is preferred. A strong signal is indicated by the ratio of 28.736. This model can be used to navigate the design space while for the trial 2, and 3 Table S2 and S3 (Supplementary material) illustrated about it with details.

3.2.2. Analysis of normal probability and perturbation plots

To identify and defend mistakes that differed from the RSM model's assumptions and predictions, the residuals are plotted using the normal probability distribution. There is no correlation between the mistakes, which have homogeneous variances and a normal distribution. The difference between actual values and those anticipated by the regression analysis is known as the residual. The residuals of the most recent RSM-BBD model are shown in Fig. 3 normal probability plot. It can be shown that the assumptions made barely violated anything. The RSM model assumptions and the residuals' independence were validated by this satisfactory normal plot of residuals. The simultaneous interaction of all independent factors and their sensitivity to the MG biosorption capacity is shown in Fig. 3. This plot fits well with the results of the ANOVA, which showed that Ag-ability MOF's to remove IBP depended mostly on variables A, B, and C.

3.2.3. Interactive effects of process parameters

To examine the influence of factors and their interactions with one another on the process response, three-dimensional (3D) plots were

Table 1

Results of an ANOVA for the parameters and response surface model for pH, conc., and dose.

Source	Sum of Squares	df	Mean Square	F-value	p-value
Model	6.14	9	0.6821	110.75	< 0.0001
A-pH	0.0149	1	0.0149	2.43	0.1633
B-Conc.	5.08	1	5.08	825.03	< 0.0001
C-Dose	0.0002	1	0.0002	0.0308	0.8656
AB	0.0029	1	0.0029	0.4786	0.5114
AC	0.0000	1	0.0000	0.0043	0.9495
BC	0.0184	1	0.0184	2.99	0.1275
A ²	0.0061	1	0.0061	0.9944	0.3519
B ²	0.9835	1	0.9835	159.68	< 0.0001
C ²	0.0069	1	0.0069	1.12	0.3247
Residual	0.0431	7	0.0062		
Lack of Fit	0.0213	3	0.0071	1.30	
Pure Error	0.0219	4	0.0055		
Cor Total	6.18	16			

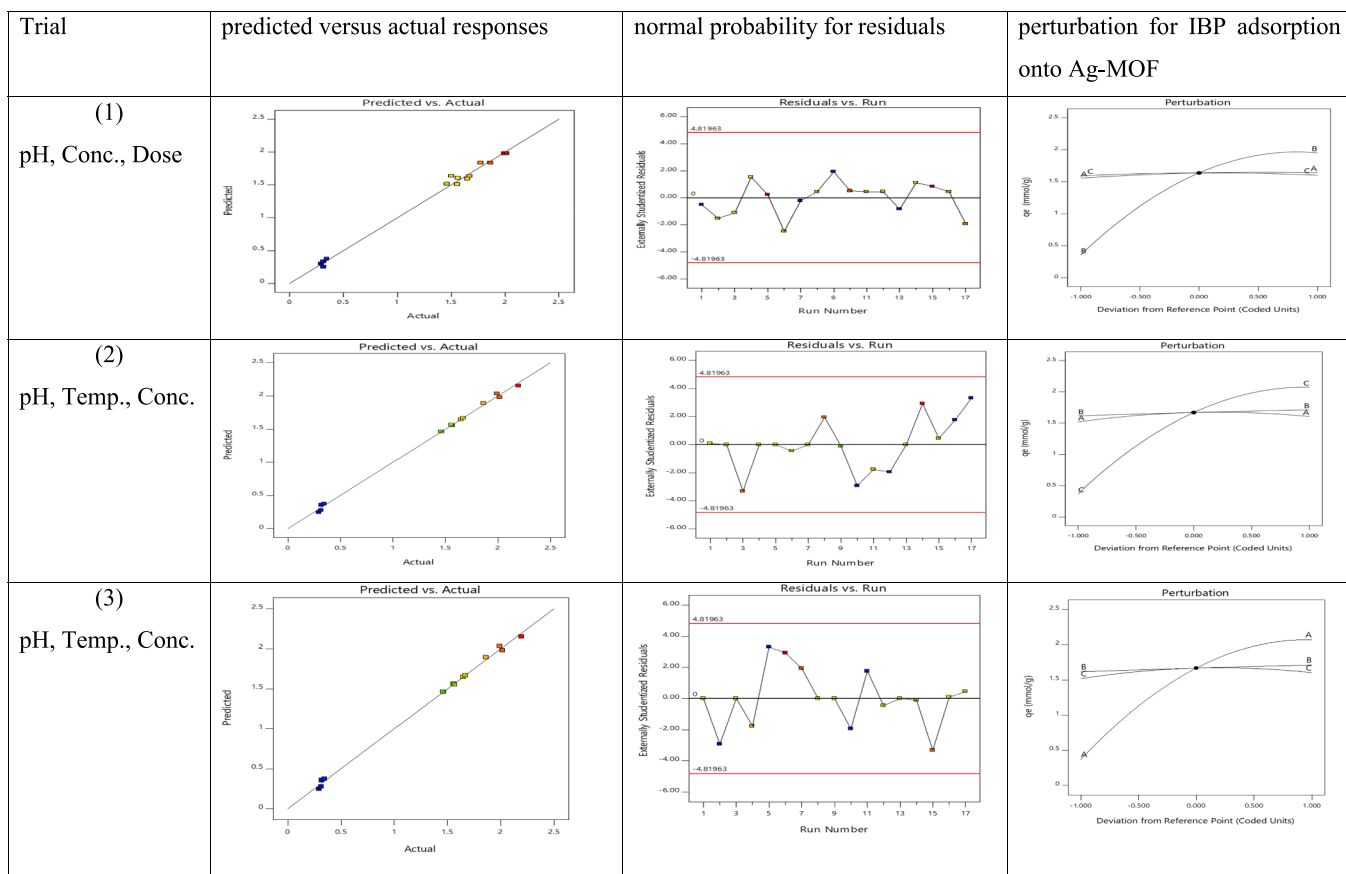


Fig. 3. Normal probability and perturbation plot.

utilized. The 3D response surface graphs were generated by the constructed quadratic model (Eq. 3). Since the model contained four independent variables and a 3D plot contains three axes, only two variables will be kept constant at the central level for each plot. Fig. 4 provides an overview of the independent variable ranges based on preliminary research. A total of 6 combined effects which are AB, AC, and BC will be discussed accordingly. The BC and AC terms in the models had statistical significance according to ANOVA. pH, Concentration, Temperature, Dose, and Time were the variables that were employed in all trials.

3.2.4. Optimization process

According to Fig. 4 at trial 1 we can find that the optimum condition will be at pH 8 with the 0.00182 mol/L, temperature 50, time 100 min, and dose 0.02 g/25 mL. Given that the adsorption capacity rose as the temperature did, these results demonstrate that the process was endothermic Fig. S4 (Supplementary material).

3.3. Batch experiments

3.3.1. The impact of pH

The pH of the dye solution must be taken into account while evaluating dye adsorption. The adsorbent's surface charge or the speciation of the adsorbate may be related to this effect (Althalhi et al., 2022). The impact of pH on the ability of Ag-MOF adsorbent to absorb MG was investigated over the pH range from (2–12). The outcomes are displayed in (Fig. 5). The impact of solution pH on MG removal (1.7×10^{-3} mol/L, 25 °C, and dosage 0.02 g/25 mL, contact time 60 min) Fig. 5(a). The findings revealed that MG's ability to adsorb to Ag-MOF adsorbent beads was pH-dependent and that the most dye could be removed under basic circumstances (between pH 8 and 12). As the pH_{ZPC} of Ag-MOF was about 8 this mean that over this pH the surface of Ag-MOF will be

have negative charge while below this pH or in acidic medium the surface will be have positive charge. During desorption the cationic dye such as MG the dye will be exhibit positive charge this led to charge transfer between the negatively charged Ag-MOF sites and the cationic groups in MG. The elimination of MG was, however, significantly reduced when the dye solution's acidity was increased. A lower concentration of cationic dye species that are available to react with the Ag-MOF active sites may be the result of a drop in dye dissociation and a decrease in adsorbent negative charge. The plot of equilibrium pH (pHeq) versus beginning pH (pH₀) is shown in Fig. 5(b). The pHeq in the basic medium had a tendency to fluctuate from its initial pH₀, as seen in the plot (Al-Hazmi et al., 2022a). The adsorption at pH₀ < 8.08 resulted in pHeq changing to become less basic, which might be due to the elimination of basic MG dye molecules from the aqueous solution (Özkar and Şengil, 2003).

3.3.2. Effect of adsorbent dose

We investigated the effect of Ag-MOF dosage on MG adsorption, and the results are provided in Fig. S1 (Supplementary material) that represented the amount of Ag-MOF used has an effect on MG adsorption: (a) Capacity of absorption vs. SD, (b) Adsorbent dose vs. relative residual concentration (C/C₀) (Al-Hazmi et al., 2022a, 2023). As the amount of Ag-MOF was increased from 0.02 to 0.25 g, the q_e of Ag-MOF gradually decreased from 2.13 mmol/L to 0.17 mmol/L. The drop in the equilibrium MG concentration with increasing dose is caused by a rise in adsorbent surface area. Active sites with a range of binding energies are present on the adsorbent's surface. All of the sites are completely exposed at the low dose of adsorbent, and the adsorption on the surface is saturated more quickly, indicating a higher adsorption capacity. Due to an excess of adsorbent for the constrained number of Ag-MOF ions in the solution, the equilibrium adsorption capacity per unit weight of the

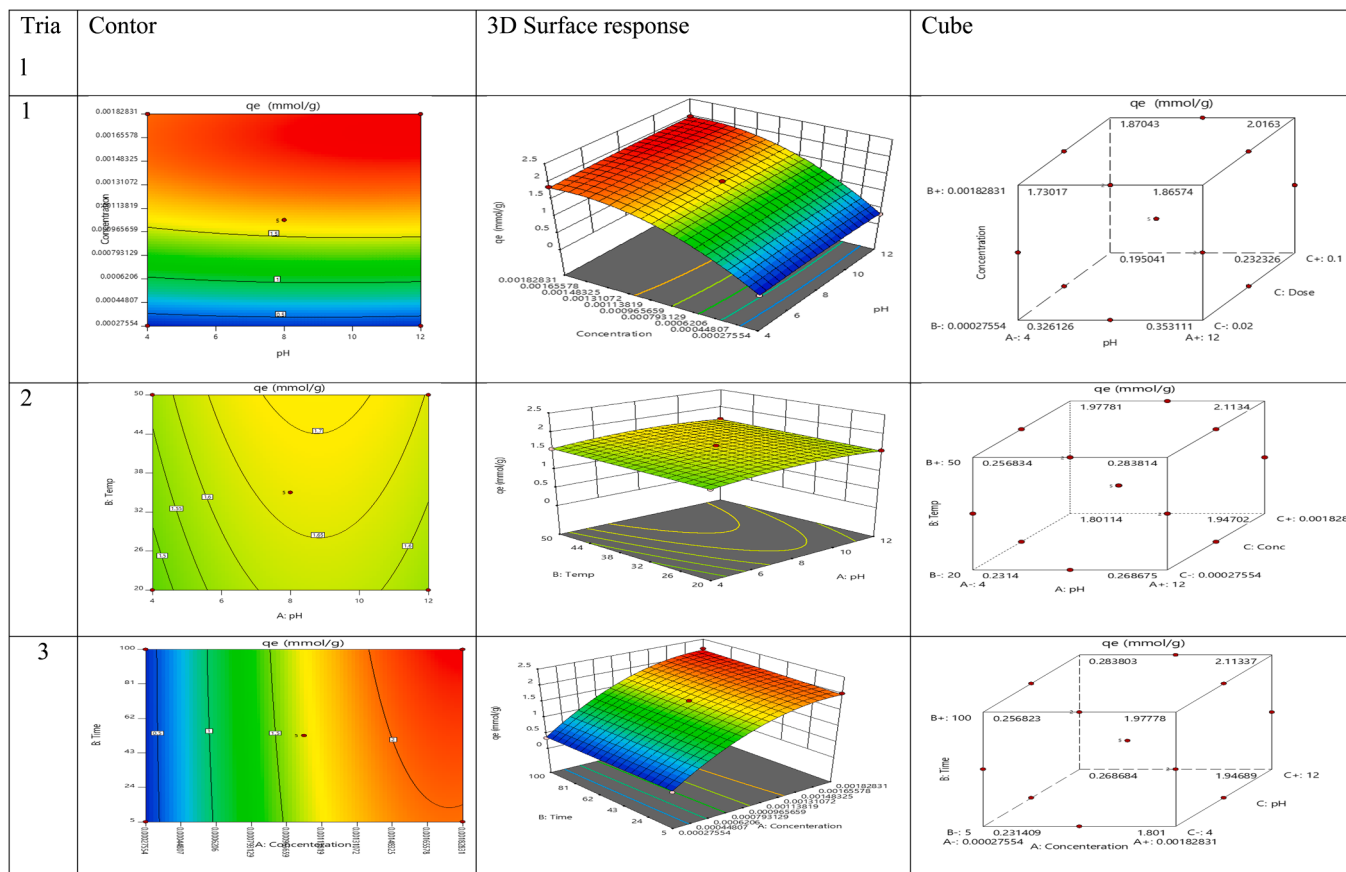
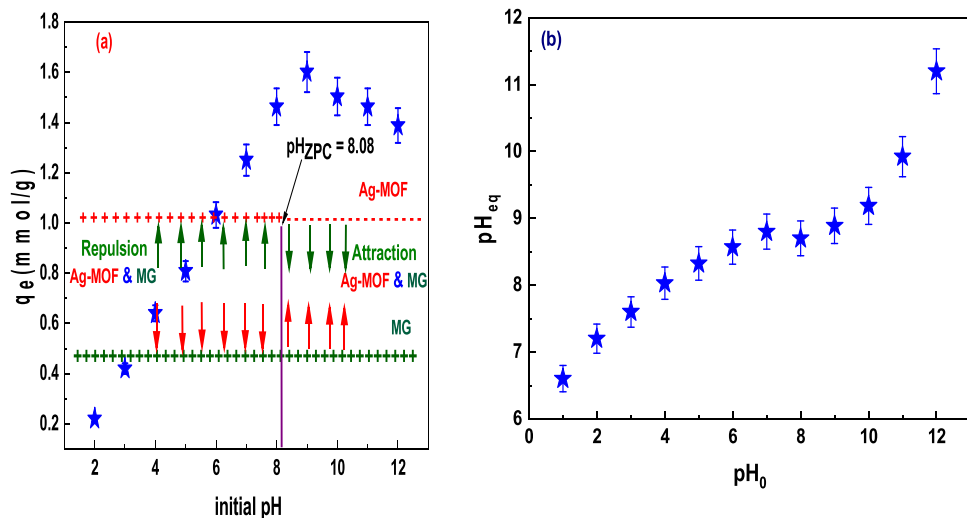


Fig. 4. 3D response surface plot for MG adsorption.

Fig. 5. (a) MG adsorption onto Ag-MOF adsorbent is affected by pH, (b) Relationship between the pH at the start of the MG adsorption process (pH_0) and the pH at equilibrium (pH_{eq}).

adsorbent (q_e) decreases as the mass of the adsorbent increases. Because increased Ag-MOF dosages gave more accessible reactive groups, the capacity of MG to adsorb in aqueous solution has been improved. On the other hand, too much adsorbent essentially limited the use of adsorption sites, which was not a good thing. According to this, Following adsorption investigations, 0.02 g Ag-MOF was determined as the optimal dosage (Djilani et al., 2015).

3.3.3. Adsorption isotherms

A sorption system's progress can be inferred from sorption isotherms, and describe the interactions between sorbent and sorbate molecules. For common adsorption Six models, namely Langmuir (Langmuir, 1917, 1918), Freundlich (Freundlich and Heller, 1939), Dubinin-Radushkevich (D-R) (Dubinin et al., 1947), Redlich-Peterson (Achmad et al., 2012), Harkin-Jura and Temkin (El-Desouky and El-Binary, 2021; El-Desouky et al., 2022). To match the experimental

data, a variety of techniques were used (Table 2). Three assumptions underlie the Langmuir model: monolayer adsorption, identical adsorption sites, and the independence of a molecule's adsorption on an adsorbent's active sites from the features of the surrounding sites' occupied (Al-Hazmi et al., 2022). In contrast, the Freundlich model is an empirical equation that typically assumes the existence of multilayer accumulation and the heterogeneous nature of the adsorbent's active sites. Temkin's model is mostly based on the linear decline of adsorption energy as opposed to the Freundlich isotherm model's proposal of an exponential decline. After the adsorption process is finished, the adsorbent saturation is also taken into consideration. The described models' linear representations are depicted in Fig. 6 and their corresponding calculated results are provided in Table 2. The examined data showed that Langmuir was more consistent with the experimental results than other isotherm models. The increased R^2 as well as agreement between the actual and theoretical loading capacity values corroborated this. All of the aforementioned experiments supported Ag-adsorbent MOF's surface's homogeneity and monolayer adsorption shape. In the Temkin model, the assumption is that the adsorption energy diminishes linearly rather than exponentially as suggested by the Freundlich pattern, taking into consideration the saturation of the adsorbent (Temkin constants of A and B). In concurrence, high A and B values of 65.25 kJ/mol, 15.093 L/mg, showed the MG dye molecules' significant interaction with the Ag-MOF adsorbent surface (Table S5) (Supplementary material). The D-R model's adsorption energy of 15.07 kJ/mol indicates that chemisorption was the method of adsorption. As 8 kJ/mol is the limit energy for distinguishing below this value this means physisorption process and the higher was chemisorption. Adaptability, a different model (Redlich-Peterson isotherm) is an improved version of; In both homogeneous and heterogeneous systems, Langmuir and Freundlich can be used. Thus, Table 2 demonstrates that, if the exponent β_R tends to zero, it confirms Freundlich isotherm model, whereas if the β_R value is close to 1, The Langmuir isotherm is obeyed. Additionally, it can be confirmed that the adsorption favours the Langmuir isotherm model based on the obtained β_R value for the adsorption of MG onto Ag-MOF (Fig. 6). The fitting coefficients in every case followed the trend. $R_L^2 > R_F^2 > R_D^2 > R_H^2$, the Langmuir model was found to be most appropriate. To put it another way, the adsorption took place primarily on a single layer (Table 2). A value of $R_L = 0$ indicates that the adsorption was irreversible; $0 < R_L < 1$ indicates that it was a good candidate for adsorption; $R_L = 1$ implies that the adsorption took place in a straight line; and $R_L > 1$ means that adsorption was not possible in

Table 2

Isothermal parameters for the adsorption of MG onto Ag-MOF adsorbent at 25 ± 1 °C.

Isotherm	Value of parameters
Langmuir	$q_m \text{ exp}$ (mmol/g)
	q_m (mmol/g)
	K_L (L/mmol)
	R_L (0.04–0.007)
Freundlich	R^2
	n
	K_F (mmol/g)(L/mmol) $^{1/n}$
Dubinin-Radushkevich	R^2
	Q_{DR}
	$K_{DR}(J^2\text{mol}^{-2})$
	Ea(kJ/mol)
Temkin	R^2
	b_T (kJ/mol)
	A_T (L/mg)
	R^2
Harkin-Jurra	A
	B
	R^2
	β
Redlich-Peterson	A
	R^2

the system. Rendering to Table 2, the R_L values (0.04–0.007) were all within the range of 0–1, implying that the adsorption procedure was successful (El-Metwaly et al., 2022).

3.3.4. Adsorption kinetics

Fig. 7 represented MG sorption kinetics; about 87 % of the MG was eliminated during the first 10 min of the quick beginning phase. When equilibrium was reached, the elimination rate was substantially slower Fig. S2 (Supplementary material). Only the PSORE model's conclusions are compatible with the simulated values (Lagergren, 1898). The linearized pseudo-second order equation revealed that the half-adsorption time, $t^{1/2}$, which is the amount of time required to reach 50 % sorbent saturation, is 3.0 min. Weber and Morris's (Intra-particle diffusion) diagram shows a linear plot (Ho and McKay, 1998). This stage of sorption is distinguished by a significantly reduced kinetic rate, which results in a gradual approach to equilibrium under the management of the resistance to intraparticle diffusion (into an interior network that is macro- and mesoporous). When sorption reached this stage, micro-pore diffusion related to intra-particle diffusion took place; k_i , X, R^2 and x^2 values were calculated and given in Table 3. X parameter provides information on the border layer's thickness; This is because the boundary layer influence on the adsorption mechanism increases with a bigger value of X. Although the exhibited linear plot did not cross through the origin, this suggests that there is a boundary layer influence. It was discovered that there is a strong connection between the experimental data and the Weber and Morris simulation line, proving that the intra-particle diffusion mechanism is suitable to explain the adsorption process of MG onto Ag-MOF (Ho and McKay, 1998). This discovery can be explained by the sorbent's extremely microporous composition. Finally, the Elovich kinetic model was employed (Zeldowitsch, 1934). The sorbent's active sites are assumed to be heterogeneous in the Elovich equation and to have a range of sorption energies (Al-Wasidi et al., 2021). It has been hypothesized that constants a and b relate to the rate of sorption and surface coverage, respectively. Table 3 presents the Elovich equation's parameters as well as the regression coefficients, R^2 . The MG sorption on the Ag-MOF sorbent has value of 2.219. (mmol/g). This number suggests that, compared to our earlier research, the initial sorption rate is significantly high, which may be explained by the sorbent's (Ag-MOF's) negative surface charge, which permitted the quick sorption of MG dye Fig. 7.

3.3.5. Adsorption thermodynamics

The adsorption process' thermodynamic coefficients (ΔH° , ΔS° and ΔG°) could be determined from Eqs. (4) and (5):

$$\Delta G^\circ = -RT \ln K_{eq} \quad (4)$$

$$\Delta G^\circ = \Delta H^\circ - T\Delta S^\circ \quad (5)$$

Eqs. (4) and (5) can be expressed as (Eq. (6)):

$$\ln K_{eq} = \frac{-\Delta H^\circ}{RT} + \frac{\Delta S^\circ}{R} \quad (6)$$

Where K_{eq} is the common equilibrium thermodynamic constant; a number of adsorption isotherms and the accompanying thermodynamic method were examined. They emphasized the significance of dimensionless form for the equilibrium constant parameters (K_{model} , for instance, the affinity constant for the Langmuir equation) Fig. S3 (Supplementary material). The connection between K_{eq} and K_{model} was also supplied. Using the Langmuir equation, the relationship (Eq. (7)) is:

$$K_{eq} = KL + \frac{C^\circ \text{ sorbate}}{\gamma \text{ sorbate}} \quad (7)$$

With coefficients of determination = 0.996, the values of ΔG° , ΔS° , and ΔH° for MG adsorption on Ag-MOF adsorbent are calculated from the Van't Hoff plot (Fig. 8). It was demonstrated that the adsorption process is spontaneous and more effective at higher temperatures

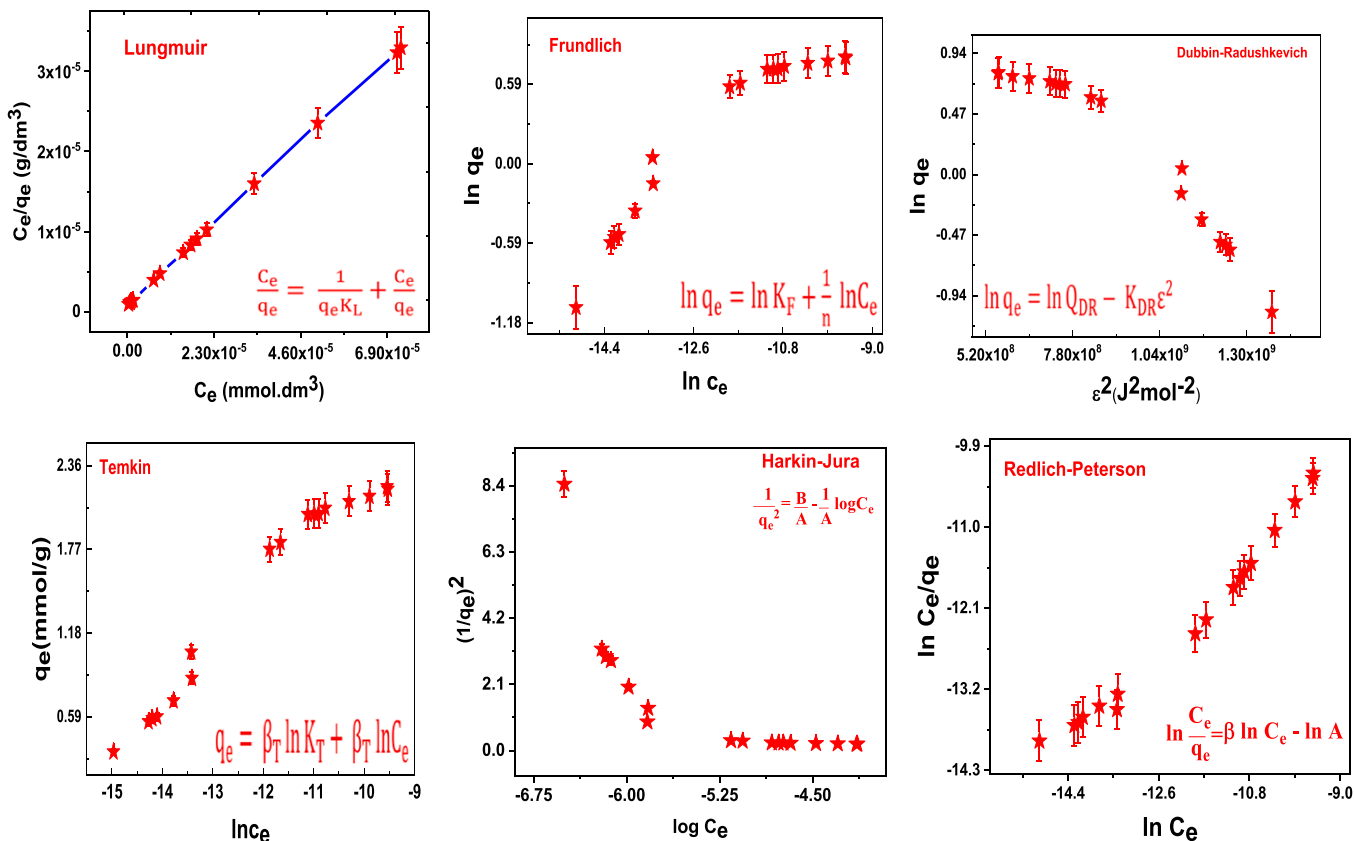


Fig. 6. Influence of MG concentrations on the adsorption process.

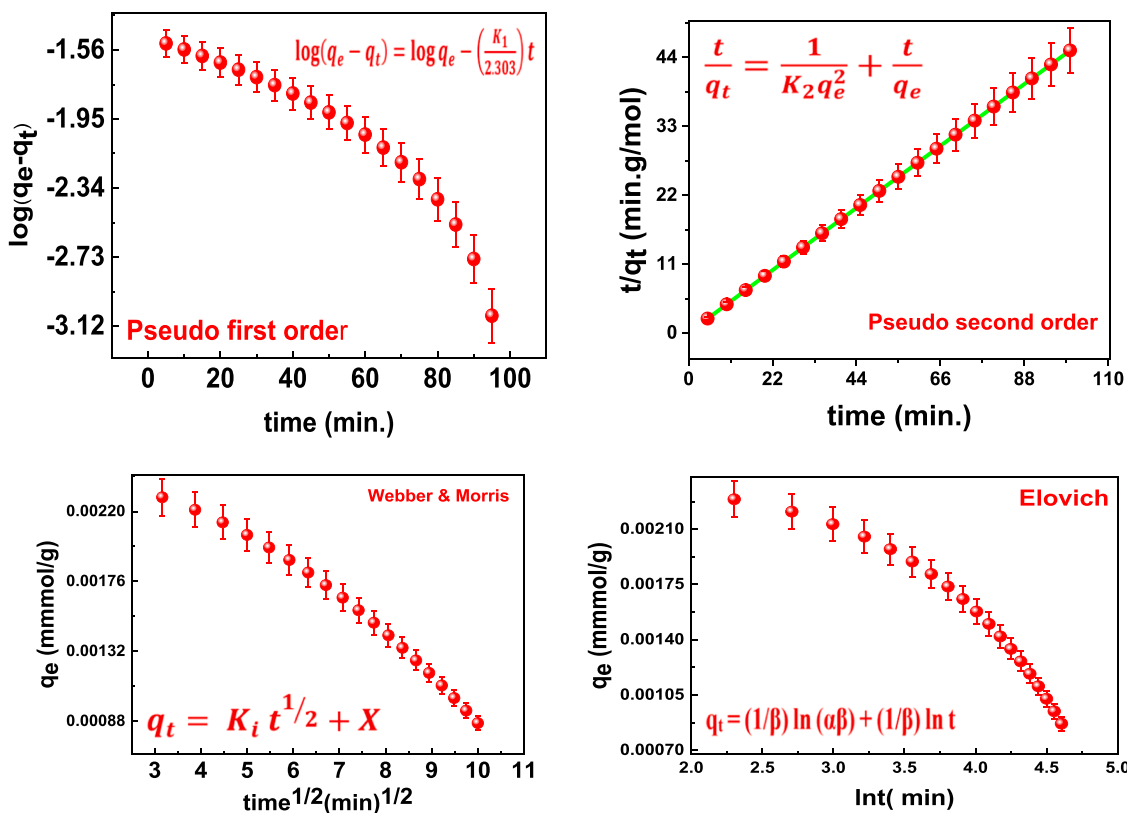


Fig. 7. Adsorption kinetic of MG on to Ag-MOF.

Table 3
Adsorption of MG onto Ag-MOF adsorbent kinetic parameters at 25 ± 1 °C.

Model	Value of parameters	
Pseudo-First-order kinetic	K_1 (min ⁻¹)	-0.0144
	q_e (mmol/g)	0.11059
	R^2	0.898
Pseudo-second-order kinetic	K_2 (g mg ⁻¹ min ⁻¹)	1.7865
	q_e (mmol/g)	2.219
	R^2	0.9999
Intraparticle diffusion	K_i (mg g ⁻¹ min ^{1/2})	-0.021
	X (mg/g)	0.0031
	R^2	0.979
Elovich	β (g/mg)	-1562.5
	α (mg g ⁻¹ min ⁻¹)	1.00405
	R^2	0.9098
Experimental data	q_e (exp) (mmol/g)	2.216

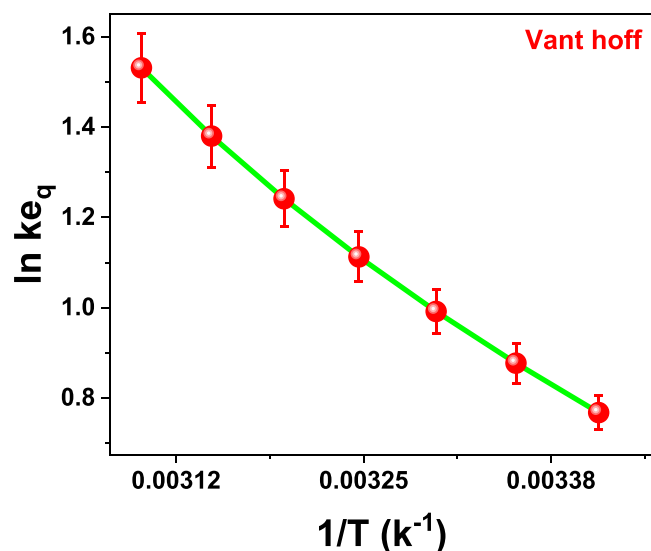


Fig. 8. Plots made by Van't Hoff for MG adsorption.

because the negative ΔG° amounts reduced as the temperature increased from 298 to 318 K (Al-Wasidi et al., 2021). The negative values of ΔG° suggest that the adsorption process is spontaneous (Table 4). The procedure is more favourable at higher temperatures within the tested temperature range, as indicated by the fact that the negative values of ΔG° climb as the temperature rises. The MG dye molecule interacts endothermically with the Ag-MOF adsorbent, as indicated by the positive value of ΔH° for MG adsorption (20.1 kJ mol⁻¹). The affirmative statement implied that even during the adsorption mechanism, the disorder or randomization at the solid-liquid interface increases. The data in Table 3 also showed that the values of $T\Delta S^\circ$ rose as the temperature rose and as $|H^\circ| < |T\Delta S^\circ|$. For this species, the adsorption reaction is characterized by a greater increase in entropy than in enthalpy (Zeldowitsch, 1934).

3.3.6. Mechanism of interaction

The electrostatic interactions between the positively charged dye ion and the negatively charged areas on the Ag-MOF surface, as well as the MG cationic dye that contain (N^+) and CH_3^+ group, may explain the

adsorption mechanism. The dye breaks down into the nitrogen ion (N^+) and chloride anion (Cl^-) in an aqueous solution. The group (OH-) at base pH may be a binding site for nitrogen ions. Ag-MOF shown good adsorption capability for both MG in a very alkaline environment, nevertheless. An approach is to use a pseudo-second-order kinetic model that relies on intra-particle diffusion. The adsorbate molecule's ionized particle properties and the early pH influence of the sorption solution on Ag-MOF nano architectonics surface chemistry may be responsible (Mirhosseini et al., 2022). The interaction energy between the charged MG molecule and the charging Ag-MOF nano architectonics surface may be the main active principle. Ag-MOF adsorbent's pH_{PZC} was determined to be 8.08 through experimental study. As the pH of the system rises, there are more negative charge positions and fewer positive charge sites. Adsorption with a negative charge rises due to electrostatic contact on the surface of the Ag-MOF nanoarchitecture. In summary (Fig. 9), the negative sites on the adsorbent and the quaternary amine on the MG are attracted to one another electrostatically; The overall adsorption mechanism of MG onto Ag-MOF adsorbent may be influenced by hydrogen bonding between the dye ring and the OH at Ag-MOF particles as well. Ag-positive MOF's cations and dye molecules' positive cations might exchange ions, and (iii) Dye adsorption on Ag-MOF may also be caused by pore filling. Because the Ag-MOF was more highly charged, there was an increase in efficiency in a very alkaline environment ($pH > pH_{PZC}$) and the higher production of OH^- made possible by the higher concentration of OH^- . The outcomes demonstrated that Ag-MOF can be used as a highly effective adsorbent to absorb cationic dye (Al-Wasidi et al., 2021).

3.3.7. Application of Ag-MOF in real water samples

In Port Said, Egypt, an effluent sample was retrieved from a nearby dyeing business. NaOH solution use to adjust the pH of the wastewater sample was brought down to 8. (0.1 M). The same procedure as for pure synthetic solutions was used for the sorption experiments: 20 mL of wastewater sample was coupled with 0.5 g of Ag-MOF sorbent for 30 min. Before and after sorption, the wastewater sample's color, pH, conductivity, and chemical oxygen demand (COD) levels were measured. Using the mass balance Eq. (2), the percent elimination of color, COD, and conductivity was computed (Al-Hazmi et al., 2022b).

Table 5 lists the sample's initial and final colors, pH, COD, and conductivity that were taken from the dyeing facility's effluent. Table 5 provides a summary of the percent deletions for various factors. Ag-MOF sorbent removes more than 95 % of color (PCU) (Platinum cobalt unit) and removes 100 % of COD. It is interesting that electrical conductivity can be effectively lowered from the wastewater sample while maintaining the initial pH of the sample.

The applicability of Ag-MOF in real environmental water samples was examined towards removal pharmaceutical effluents such as diclofenac sodium (DCF) So, during spike the three samples of water Pure, Domestic, and lack with 20 mg/L of DCF at different pH 2, 6, and 10, temperature 25 °C, and time 90 min the results were illustrated at the Fig. 4 S (a) and the optimum removal were at pH 6 as the follow 98.6, 98.2, and 96.4 for water Pure, Domestic, and lack, respectively.

And on other hand at the same conditions tested the efficiency of the Ag-MOF towards removal different non-steroidal anti-inflammatory drugs (NSAIDs) such as Naproxen (NPX), Ketoprofen (KP), Aspirin (ASA), and Ibuprofen (IPB) by spike the pure water with 20 mg/L and the results was illustrated at Fig. S4 (b) (Supplementary material).

Table 4
Thermodynamic factors affecting the MG adsorption onto the Ag-MOF adsorbent.

Adsorbate	ΔH° (kJ/mol)	ΔS° (J/mol K)	T_0 (K)	$-\Delta G^\circ$ (kJ/mol)				
				293 K	298 K	303 K	308 K	318 K
MG	20.1	78.04	288.68	1.92	2.27	2.64	2.96	3.75

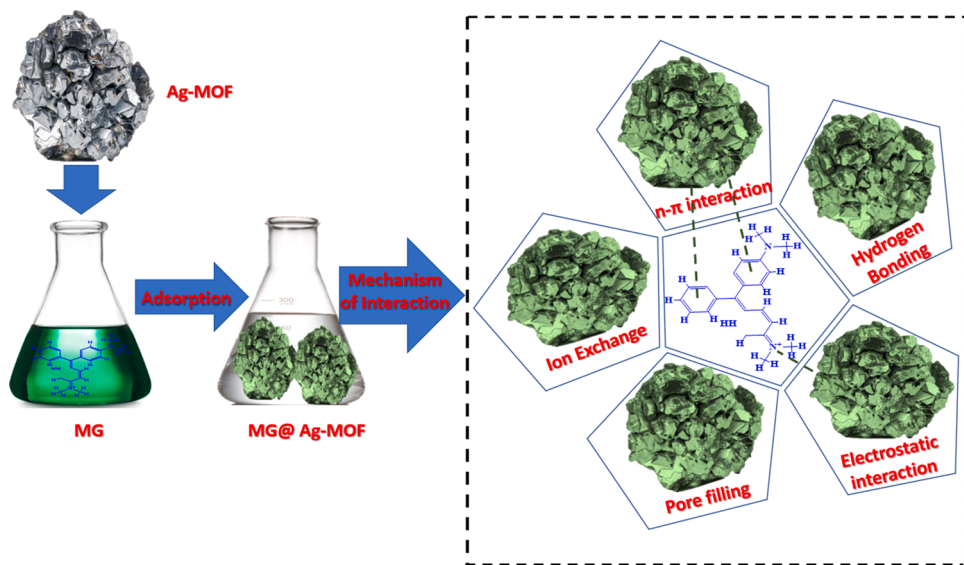


Fig. 9. Ag-MOF removes MG from an aqueous solution using an adsorption process.

Table 5
The use of an Ag-MOF adsorbent to remove color from real wastewater samples.

Parameter	Unit	Before adsorption	After Adsorption	%Removal
pH	–	7.8	8.5	–
Conductivity	µS/cm	932	806	13.6
Color	PCU	979	16	98.36
COD	–	432	18	95.83

3.3.8. Reusability of the Ag-MOF for MG removal

The obtained regeneration efficiency (%) was found to be 98.6 %, 93.4 %, 87.8 %, 85.4 %, and 82.7 % for five consecutive cycles of adsorption and desorption. The little reduction in regenerating effectiveness might be due to some Ag-MOF adsorption sites being relatively blocked off. This result shows that the recycling rate of Ag-MOF adsorbent is high. Eq. 8's regeneration effectiveness was utilized to calculate:

$$\text{Regeneration efficiency (\%)} = \frac{\text{Amount of desorbed MG into the elution solution}}{\text{Amount of adsorbed MG (mmol)}} \times 100 \quad (8)$$

Using an atomic absorption spectrophotometer, the liberated silver from Ag-MOF during the desorption process was examined (iCE 3300 AAS Atomic Absorption Spectrometer, Thermo Fisher Scientific, USA). There are a variety of outcomes for the Ag release from the Ag-MOF adsorbent to the eluent solution Ag was 0.13 mg/L and 0.19 mg/L. This result shows that the adsorbent is retaining its stability during the regeneration process.

3.3.9. Effect of salinity

Whenever dying fabric using reactive or cationic dyes, large amounts of salts are frequently utilized. Inside sewage, Na^+ and Cl^- The majority of them have dyed anions and cations. As they are now present in this system, the Ag-MOF surface and the MG ion have an alluring relationship when it comes to electrostatic interactions. With increasing ionic strength, the adsorption capacity should decrease. Fig. S5 (Supplementary material) demonstrates how the Cl^- affects MG removal by Ag-MOF

adsorbent. The MG adsorption was decreased whenever NaCl was added to the MG solution. By increasing the salt concentration, the colours' fading was slowed. This effect was apparent even at low NaCl levels in the dye solution. This outcome can be explained by the interactions between the surface and the extra solutes, which may prevent some of the dye molecules from adsorbing at their active sites. The hydrated ion radius may interfere with the electrostatic interaction between the quaternary ammonium cation on the dye and the negative charge on Ag-MOF since larger contaminants can compete with Na^+ ions with smaller ion radii. Ag-ability MOF's to absorb dye is reduced when molecules, such MG molecules, are placed on its surface.

3.3.10. MG dye adsorption with different adsorbents: comparison

Table 6 compares the maximum adsorption capacities of the Ag-MOF with various values from the literature as well as the optimal operating conditions. However, this is a good criterion for broadly evaluating the

potential of these materials. Direct comparison of sorption performance is difficult due to different experimental setups. The Ag-MOF adsorbent provides a substantial advantage related to its quick kinetics, which must be emphasized. The ability of Ag-adsorbents MOF's to efficiently absorb MG dye suggests that they may have use in the removal of MG dye from wastewater.

3.3.11. In vitro anti-microbial activity

A well-diffused technique is used to measure the antifungal and antibacterial activity of ethanol extracts from Ag-MOF against ethanol extracts from *Candida albicans*, *Staphylococcus aureus*, and *Escherichia coli* Ag-MOF. Table S6 (Supplementary material) represented the efficiency of the Ag-MOF towards Fungus, Gram positive and negative bacteria.

4. Conclusion

The indirect discharge of considerable quantities of poisonous dyes

Table 6Adsorption efficiency (q_m) for the MG dye, of several adsorbents.

Adsorbent	pH	C_i	Time (min.)	q_e (mg/g)	Reference
Cellulose	7.2	50	30	2.4	(Sekhar et al., 2009)
Pithophora sp. (algae)	5	100	300	117.6	(Vasanth Kumar et al., 2005)
Aerobic granules	2–11	80	120	56.8	(Sun et al., 2008)
Chlorella sp. (algae)	78	10	60	33.6	(Tsai and Chen, 2010)
Walnut shell	5	100	120	90.8	(Dahri et al., 2014)
Spent tea leaves	4	100	180	256.4	(Akar et al., 2013)
Caulerpa racemosa (algae)	6	60	300	25.67	(Bekçi et al., 2009)
Potato peel	4	50	210	35.61	(Guechi and Hamdaoui, 2016)
Solanum tuberosum wastes	7	10	21	33.3	(Gupta et al., 2016)
Clayey soil	6	50	360	78.57	(Vickers, 2017)
Bacillus cereus M116	5	100	360	485	(Nath and Ray, 2015)
Ag-MOF	8	100	100	802.78	This work

into water has had a negative influence on ecosystem. So, in this research, an environmentally friendly mesoporous inorganic-organic Ag metal-organic framework was used to investigate a way to remove colours from industrial water (MOFs). The Ag-MOF was able to extract MG dye from wastewater thanks to intergrowing chains that had uniform micropore sizes and highly accessible surface areas. The inorganic-organic frameworks shown a superb capability for MG adsorption. The Ag-MOF adsorbent's ability to generate an active negatively charged surface was significantly influenced by the adsorption conditions, such as the pH of the solution, resulting in surfaces that are very capable of interacting with and absorbing MG dye. Adsorption tests showed that Ag-MOF had a good capacity for MG elimination (809.7 mg g^{-1}), and even after several reuse cycles, its capability remained intact. The PSORE model was used to fit the MG adsorption process onto Ag-MOF, and it was proportional to Langmuir theory. Mechanisms of sorption may be involved: (i) Forces of electrostatic attraction, (ii) hydrogen bonding (iii) $n-\pi$ stacking attraction. Thermodynamics evaluation for sorption processes, this is in good agreement with the measured sorption. Endothermic adsorption is indicated by isotherms. The inclusion of NaCl has only a little effect on the adsorption capabilities (up to 40 g/L) due to charge screening and chloride ion competition. Furthermore, the desorption efficiency of the Ag-MOF as planned was > 91.6 % after 6 adsorption/desorption cycles in a row. The mesoporous Ag-MOF adsorbent offered an easy and effective way to handle industrial effluent and water filtering. The removal of MG dye from wastewater samples using Ag-MOF adsorbents is described in this work, which, in our opinion, is a first. On the other hand, Ag-MOF is effective against both Gram positive and negative bacteria as well as fungus.

Declaration of Competing Interest

The authors declare that they have no known competing financial interests or personal relationships that could have appeared to influence the work reported in this paper.

Acknowledgments

Princess Nourah bint Abdulrahman University Researchers Supporting Project number (PNURSP2023R122), Princess Nourah bint Abdulrahman University, Riyadh, Saudi Arabia.

Appendix A. Supporting information

Supplementary data associated with this article can be found in the online version at doi:10.1016/j.psep.2023.02.036.

References

- Abdolali, A., Guo, W., Ngo, H., Chen, S., Nguyen, N., Tung, K., 2014. Typical lignocellulosic wastes and by-products for biosorption process in water and wastewater treatment: a critical review. *J. Bioresour. Technol.* 160, 57–66.
- Achmad, A., Kassim, J., Suan, T.K., Amat, R.C., Seey, T.L., 2012. Equilibrium, kinetic and thermodynamic studies on the adsorption of direct dye onto a novel green adsorbent developed from Uncaria gambir extract. *J. Phys. Sci.* 23, 1–13.
- Adebayo, M.A., Prola, L.D., Lima, E.C., Puchana-Rosero, M., Cataluña, R., Saucier, C., Umpierrez, C.S., Vaghetti, J.C., da Silva, L.G., Ruggiero, R.J., 2014. Adsorption of Procion Blue MX-R dye from aqueous solutions by lignin chemically modified with aluminium and manganese. *J. Hazard. Mater.* 268, 43–50.
- Agarwal, M., Singh, K., 2017. Heavy metal removal from wastewater using various adsorbents: a review. *J. Water Reuse Desalin.* 7, 387–419.
- Akar, E., Altinişik, A., Seki, Y., 2013. Using of activated carbon produced from spent tea leaves for the removal of malachite green from aqueous solution. *J. Ecol. Eng.* 52, 19–27.
- Al-Hazmi, G.A., El-Zahhar, A.A., El-Desouky, M.G., El-Binary, A., 2022. Superior Adsorption and removal of doxorubicin from aqueous solution using activated carbon via thermally treated green adsorbent: isothermal, kinetic, and thermodynamic studies. *J. Environ. Technol.* 1–47.
- Al-Hazmi, G.A., El-Zahhar, A.A., El-Desouky, M.G., El-Binary, M.A., El-Binary, A.A., 2022b. Adsorption of industrial dye onto a zirconium metal-organic framework: synthesis, characterization, kinetics, thermodynamics, and DFT calculations. *J. Coord. Chem.* 1–27.
- Al-Hazmi, G.H., El-Desouky, M.G., El-Binary, A.A., 2022a. Synthesis, characterization and microstructural evaluation of ZnO nanoparticles by William-Hall and size-strain plot methods. *Bull. Chem. Soc. Ethiop.* 36, 815–829.
- Al-Hazmi, G.H., Adam, A.M.A., El-Desouky, M.G., El-Binary, A.A., Alsuhaibani, A.M., Refat, M.S., 2023. Efficient adsorption of Rhodamine B using a composite of Fe3O4@zif-8: Synthesis, characterization, modeling analysis, statistical physics and mechanism of interaction. *Bull. Chem. Soc. Ethiop.* 37, 211–229.
- Al-Hazmi, Gamil A.A., El-Binary, Mohamed A., El-Desouky, Mohamed G., El-Binary, A.A., 2022a. Efficient adsorptive removal of industrial dye from aqueous solution by synthesized zeolitic imidazolate framework-8 loaded date seed activated carbon and statistical physics modeling. *Desalin. Water Treat.* 258, 85–103.
- Altalhi, T.A., Ibrahim, M.M., Mersal, G.A., Mahmoud, M., Kumeria, T., El-Desouky, M.G., El-Binary, A.A., El-Binary, M.A., 2022. Adsorption of doxorubicin hydrochloride onto thermally treated green adsorbent: Equilibrium, kinetic and thermodynamic studies. *J. Mol. Struct.* 1263, 133160.
- Al-Wasidi, A.S., AlZahrani, I.I.S., Thawibaraka, H.I., Naglah, A.M., El-Desouky, M.G., El-Binary, M.A., 2021. Adsorption studies of carbon dioxide and anionic dye on green adsorbent. *J. Mol. Struct.* 1250, 131736.
- Al-Wasidi, A.S., AlZahrani, I.I.S., Naglah, A.M., El-Desouky, M.G., Khalil, M.A., El-Binary, A.A., El-Binary, M.A., 2021. Effective removal of methylene blue from aqueous solution using metal-organic framework; modelling analysis, statistical physics treatment and DFT calculations. *ChemistrySelect* 6, 11431–11447.
- Amarasoriya, A., Kawakami, T., 2019. Removal of fluoride, hardness and alkalinity from groundwater by electrolysis. *J. Groundw. Sustain. Dev.* 9, 100231.
- Arjmand, O., Arjmand, M., Amani, A.M., Eikani, M.H., 2020. Effective adsorption of doxorubicin hydrochloride on green magnetic/graphene oxide/chitosan/allium sativum/quercus/nanocomposite. *Acta Chim. Slov.* 67, 496–506.
- Bekçi, Z., Seki, Y., Cavas, L., 2009. Removal of malachite green by using an invasive marine alga Caulerpa racemosa var. cylindracea. *J. Hazard. Mater.* 161, 1454–1460.
- Celik, S., Duman, N., Sayin, F., Akar, S.T., Akar, T.J., 2021. Microbial cells immobilized on natural biomatrix as a new potential ecofriendly biosorbent for the biotreatment of reactive dye contamination. *J. Water Process Eng.* 39, 101731.
- Dahri, M.K., Kooh, M.R.R., Lim, L.B., 2014. Water remediation using low cost adsorbent walnut shell for removal of malachite green: equilibrium, kinetics, thermodynamic and regeneration studies. *J. Environ. Chem. Eng.* 2, 1434–1444.
- Djalani, C., Zaghdoudi, R., Djazi, F., Bouchekima, B., Lallam, A., Modarressi, A., Rogalski, M., 2015. Adsorption of dyes on activated carbon prepared from apricot stones and commercial activated carbon. *J. Taiwan Inst. Chem. Eng.* 53, 112–121.
- Dubinin, M., Zaverina, E.D., Radushkevich, L.V., 1947. Sorption and structure of active carbons I. Adsorption of organic vapors. *Zh. Fiz. Khimii* 21, 1351–1362.
- El-Desouky, M.G., El-Binary, A.A., 2021. Magnetic metal-organic framework (Fe3O4@ZIF-8) nanocomposites for adsorption of anionic dyes from wastewater. *Inorg. Nano-Met. Chem.* 1–15.
- El-Desouky, M.G., El-Binary, A.A., El-Binary, M.A., 2021. Low-temperature adsorption study of carbon dioxide on porous magnetite nanospheres iron oxide. *Biointerface Res. Appl. Chem.* 12, 6252–6268.
- El-Desouky, Mohamed G., Khalil, Muhammad A., El-Binary, Ashraf A., ElBinary, M.A., 2022. Biological, biochemical and thermochemical techniques for biofuel production: an updated review. *Biointerface Res. Appl. Chem.* 12, 3034–3054.
- El-Desouky, M.G., El-Binary, M.A., El-Binary, A.A., 2021. Effective adsorptive removal of anionic dyes from aqueous solution. *Vietnam J. Chem.* 59, 341–361.
- El-Metwaly, N.M., Katouah, H.A., El-Desouky, M., El-Binary, A., El-Binary, M., 2023. Fabricating of Fe3O4@ Ag-MOF nanocomposite and evaluating its adsorption activity for removal of doxorubicin. *J. Environ. Sci. Health, Part A*, 57, 1099–1115.

- El-Sewify, I.M., Radwan, A., Shahat, A., El-Shahat, M., Khalil, M.M.J.M., 2022. Superior adsorption and removal of aquaculture and bio-staining dye from industrial wastewater using microporous nanocubic Zn-MOFs. *J. Microporous Mesoporous Mater.* 329, 111506.
- El-Subruti, G., Eltaweil, A., Sallam, S., 2019. Synthesis of active MFe₂O₄/γ-Fe₂O₃ nanocomposites (metal= Ni or Co) for reduction of nitro-containing pollutants and methyl orange degradation. *J. Nano* 14, 1950125.
- Freundlich, H., Heller, W., 1939. The adsorption of cis-and trans-azobenzene. *J. Am. Chem. Soc.* 61, 2228–2230.
- Fuglie, J., Källne, E., Watson, L., Fabian, D., 1977. Electronic structure of aluminum and aluminum-noble-metal alloys studied by soft-x-ray and x-ray photoelectron spectroscopies. *Phys. Rev. B* 16, 750.
- Gao, J.-F., Zhang, Q., Wang, J.-H., Wu, X.-L., Wang, S.-Y., Peng, Y.-Z., 2011. Contributions of functional groups and extracellular polymeric substances on the biosorption of dyes by aerobic granules. *J. Bioresour. Technol.* 102, 805–813.
- Garg, D., Kumar, S., Sharma, K., Majumder, C., 2019. Application of waste peanut shells to form activated carbon and its utilization for the removal of Acid Yellow 36 from wastewater. *J. Groundw. Sustain. Dev.* 8, 512–519.
- Gu, S.H., Nicolas, V., Lalíš, A., Sathirapongsasuti, N., Yanagihara, R.J.I., 2013. Genetics, Complete genome sequence and molecular phylogeny of a newfound hantavirus harbored by the Doucet's musk shrew (*Crocidura douceti*) in Guinea. *J. Infect., Genet. Evol.* 20, 118–123.
- Guechi, E.-K., Hamdaoui, O., 2016. Sorption of malachite green from aqueous solution by potato peel: kinetics and equilibrium modeling using non-linear analysis method. *J. Arab. J. Chem.* 9, S416–S424.
- Gupta, N., Kushwaha, A.K., Chattopadhyaya, M., 2016. Application of potato (*Solanum tuberosum*) plant wastes for the removal of methylene blue and malachite green dye from aqueous solution. *J. Arab. J. Chem.* 9, S707–S716.
- Hassan, N., Shahat, A., El-Didamony, A., El-Desouky, M.G., El-Binary, A.A., 2020. Mesoporous iron oxide nano spheres for capturing organic dyes from water sources. *J. Mol. Struct.* 1217, 128361.
- Ho, Y.-S., McKay, G., 1998. Sorption of dye from aqueous solution by peat. *Chem. Eng. J.* 70, 115–124.
- Islam, M., Mostafa, M., 2018. Textile dyeing effluents and environment concerns-a review. *J. Environ. Sci. Nat. Resour.* 11, 131–144.
- Kim, H.-G., Choi, K., Lee, K., Lee, S., Jung, K.-W., Choi, J.-W., 2021. Controlling the Structural Robustness of Zirconium-Based Metal Organic Frameworks for Efficient Adsorption on Tetracycline Antibiotics. *Water* 13, 1869.
- S. Lagergren, Zur theorie der sogenannten adsorption gelöster stoffe, 1898.
- Langmuir, I., 1917. The constitution and fundamental properties of solids and liquids. II. Liq. *J. Am. Chem. Soc.* 39, 1848–1906.
- Langmuir, I., 1918. The adsorption of gases on plane surfaces of glass, mica and platinum. *J. Am. Chem. Soc.* 40, 1361–1403.
- Lee, C., Low, K., Gan, P., 1999. Removal of some organic dyes by acid-treated spent bleaching earth. *J. Environ. Technol.* 20, 99–104.
- Li, Q., Zhang, C., Tan, W., Gu, G., Guo, Z., 2017. Novel amino-pyridine functionalized chitosan quaternary ammonium derivatives: Design, synthesis, and antioxidant activity. *J. Mol.* 22, 156.
- Mahmoodi, N.M., 2013. Photodegradation of dyes using multiwalled carbon nanotube and ferrous ion. *J. Environ. Eng.* 139, 1368–1374.
- H. Mirhosseini, T. Shamsipur, A.J.A.O.C. Mostafavi, Novel adsorbent g-C₃N₄/ZnV₂O₄ for efficient removal of crystal violet dye: Removal process optimization, adsorption isotherms, and kinetic modeling, 36, 2022, p. e6867.
- Mohammad Mahmoodi, Niyaz, 2013. Nickel Ferrite Nanoparticle: Synthesis, Modification by Surfactant and Dye Removal Ability. *J. Water Air Soil Pollut.* 224, 1–8.
- Nath, J., Ray, L., 2015. Biosorption of Malachite green from aqueous solution by dry cells of *Bacillus cereus* M116 (MTCC 5521). *J. Environ. Chem. Eng.* 3, 386–394.
- Özcar, M., Şengil, İ.A., 2003. Adsorption of reactive dyes on calcined alunite from aqueous solutions. *J. Hazard. Mater.* 98, 211–224.
- Prabhu, S.M., Kancharla, S., Park, C.M., Sasaki, K., 2019. Synthesis of modulator-driven highly stable zirconium-fumarate frameworks and mechanistic investigations of their arsenite and arsenate adsorption from aqueous solutions. *CrystEngComm* 21, 2320–2332.
- Rashid, A., Khan, S., Ayub, M., Sardar, T., Jehan, S., Zahir, S., Khan, M.S., Muhammad, J., Khan, R., Ali, A., 2019. Mapping human health risk from exposure to potential toxic metal contamination in groundwater of Lower Dir, Pakistan: application of multivariate and geographical information system. *J. Chemosphere* 225, 785–795.
- Royer, B., Cardoso, N.F., Lima, E.C., Vaghetti, J.C., Simon, N.M., Calvete, T., Veses, R.C., 2009. Applications of Brazilian pine-fruit shell in natural and carbonized forms as adsorbents to removal of methylene blue from aqueous solutions—Kinetic and equilibrium study. *J. Hazard. Mater.* 164, 1213–1222.
- Sallam, S., El-Subruti, G., Eltaweil, A., 2018. Facile synthesis of Ag-γ-Fe₂O₃ superior nanocomposite for catalytic reduction of nitroaromatic compounds and catalytic degradation of methyl orange. *J. Catal. Lett.* 148, 3701–3714.
- Sekhar, C.P., Kalidhasan, S., Rajesh, V., Rajesh, N., 2009. Bio-polymer adsorbent for the removal of malachite green from aqueous solution. *J. Chemosphere* 77, 842–847.
- Sun, X.-F., Wang, S.-G., Liu, X.-W., Gong, W.-X., Bao, N., Gao, B.-Y., Zhang, H.-Y., 2008. Biosorption of Malachite Green from aqueous solutions onto aerobic granules: kinetic and equilibrium studies. *J. Bioresour. Technol.* 99, 3475–3483.
- Tsai, W.-T., Chen, H.-R., 2010. Removal of malachite green from aqueous solution using low-cost chlorella-based biomass. *J. Hazard. Mater.* 175, 844–849.
- Vasantha Kumar, K., Sivanesan, S., Ramamurthy, V., 2005. Adsorption of malachite green onto *Pithophora* sp., a fresh water algae: Equilibrium and kinetic modelling. *J. Process Biochem.* 40, 2865–2872.
- Vickers, N.J., 2017. Animal communication: when i'm calling you, will you answer too? *J. Curr. Biol.* 27, R713–R715.
- Wang, Y., Li, L., Dai, P., Yan, L., Cao, L., Gu, X., Zhao, X., 2017. Missing-node directed synthesis of hierarchical pores on a zirconium metal-organic framework with tunable porosity and enhanced surface acidity via a microdroplet flow reaction. *J. Mater. Chem. A* 5, 22372–22379.
- Zeldowitsch, J., 1934. Über den mechanismus der katalytischen oxydation von CO an MnO₂. *Acta physicochim URSS* 1, 364–449.